Chemical Engineering Journal 362 (2019) 897–908

Contents lists available at ScienceDirect

Chemical Engineering Journal

journal homepage: www.elsevier.com/locate/cej

Complete degradation of bisphenol A and nonylphenol by a composite of biogenic manganese oxides and *Escherichia coli* cells with surface-displayed multicopper oxidase CotA

Zhen Zhang[a,d], Zhiyong Ruan[b], Jin Liu[a], Chang Liu[a], Fuming Zhang[c], Robert J. Linhardt[c], Lin Li[a,*]

[a] State Key Laboratory of Agricultural Microbiology, Huazhong Agricultural University, Wuhan 430070, PR China
[b] Key Laboratory of Microbial Resources, Ministry of Agriculture, Institute of Agricultural Resources and Regional Planning, CAAS, Beijing 100081, PR China
[c] Department of Chemistry and Chemical Biology, Center for Biotechnology and Interdisciplinary Studies, Rensselaer Polytechnic Institute, Troy, NY 12180, USA
[d] College of Food and Bioengineering, Henan University of Animal Husbandry and Economy, Zhengzhou 450046, PR China

HIGHLIGHTS

- A composite of biogenic Mn oxide and engineered bacterium for dual degradation.
- Complete degradation of representative EDCs and elimination of oestrogenic toxicity.
- Synergistic adsorption and multiple oxidative degradations.
- High repeatability and regeneration with potential for continuous operation.

GRAPHICAL ABSTRACT

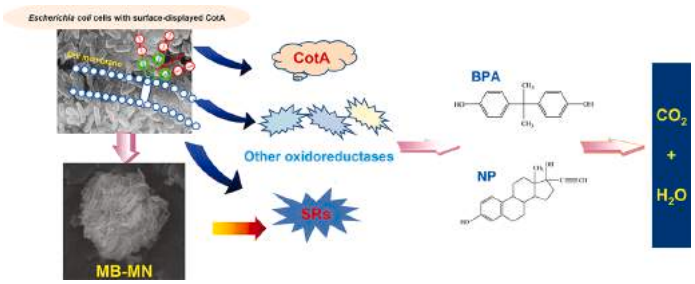

ARTICLE INFO

Keywords:
Endocrine-disrupting chemical
Biodegradation
Spore coat protein A
Manganese oxide
Cell surface display technology

ABSTRACT

Endocrine-disrupting chemicals (EDCs) are a large group of environmental toxicants that pose serious risks to public health. In this study, we report a new method for the complete degradation of EDCs using a dual oxidation-action composite of biogenic manganese oxides and engineered *Escherichia coli* cells with surface-expressed multicopper oxidase CotA. The *cotA* gene from a Mn^{2+}-oxidizing bacterium was constructed as a fusion gene "*inaQ-N/cotA*" with an anchoring motif *inaQ-N* from *Pseudomonas syringae* and was expressed in *E. coli* cells to display catalytic CotA on the cell surface. Under prolonged Mn^{2+}-enriched culturing conditions, the engineered cells were capable of forming microspherical aggregated composites that were mainly composed of ramsdellite (MnO_2). The ability of the composite to degrade two EDCs, bisphenol A (BPA) and nonylphenol (NP), was investigated. GC–MS assays identified 7 and 10 degraded intermediates using the ^{13}C isotope from ^{13}C-labeled BPA and ^{13}C-labeled NP, respectively. The appearance of $^{13}CO_2$ from both reaction mixtures revealed mineralization pathways of BPA and NP by this composite. Bioassays using *Caenorhabditis elegans* as an indicator organism demonstrated that the estrogenic activity of BPA and NP was eliminated by these degradation processes. The reaction of the composite proceeded at an acidic pH and room temperature. A consecutive three-round treatment process showed comparable levels of degradation by the composite in repeated reactions and showed that the activity could be easily recovered. Moreover, the superoxide radical levels of BPA-degradation and NP-degradation were monitored during the 24 h reaction time, and possible BPA-degradation and NP-degradation pathways by the composite were proposed.

* Corresponding author at: State Key Laboratory of Agricultural Microbiology, Huazhong Agricultural University, Wuhan 430070, Hubei Province, PR China.
E-mail address: lilin@mail.hzau.edu.cn (L. Li).

https://doi.org/10.1016/j.cej.2019.01.062
Received 9 November 2018; Received in revised form 5 January 2019; Accepted 11 January 2019
Available online 14 January 2019
1385-8947/

1. Introduction

Endocrine-disrupting chemicals (EDCs) are a large group of widespread substances that exert potentially adverse health effects by mimicking endogenous hormones in affected organisms [1]. High levels of EDCs cause serious endocrine, reproductive or neurological problems in humans and wildlife [2,3]. Exposure to moderate levels of EDCs also elicits abnormal responses that occur at inappropriate times or can block the functions of normal hormones [4]. Even trace levels of EDCs lead to sustained estrogenic effects; for example, a very pronounced increase in vitellogenin was observed in trout plasma exposed to certain effluents containing trace levels (ng L^{-1}) of 17β-estradiol (E2) or 17α-ethynylestradiol (EE2) [5]. Due to the common use of EDCs, these toxicants are often found in various surface water and wastewater effluents [6] and ultimately accumulate in humans through the food chain.

Over the past decade, intensive efforts have been undertaken to develop effective processes for the treatment of EDCs in wastewater effluents or other environments [7]. Physiochemical methods, such as adsorption, membrane-based filtration, and electrochemical and photochemical degradation, have been studied. However, these methods have generally been considered to be ineffective or too expensive [7,8]. Biological processes based on microbial enzymes or bioactive materials are increasingly appealing alternatives because of their high biodegradability, cost-effectiveness and environmental friendliness [9]. The effective biodegradation of EDCs by a variety of microorganisms and their enzymes have been reported, including a purified laccase from the fungus *Trametes villosa* that degrades bisphenol A (BPA) [10], a heterologously expressed laccase from *Irpex lacteus* that treats nonylphenol (NP) [11], and a manganese peroxidase that degrades BPA and NP [12]. Even at low EDC concentrations, the degradation achieved by microorganisms or enzymes was superior compared with other treatments [13]. However, studies of the complete degradation of EDCs by microbial enzymes have been limited. Some studies have observed substantial residual or even transiently increased estrogenic activity during EDC decomposition by microbes or modifying enzymes [1,14].

Manganese oxides (Mn oxides in brief) are natural catalysts and adsorbents with high redox potential and high adsorptive capacities [15]. They can remove organic or inorganic contaminants, such as phenols, chlorinated phenols, chlorinated anilines, atrazine, and a variety of inorganics [16,17]. Abiotic Mn dioxides have been previously used to oxidize BPA [18], E2 [19], estrone, estriol and EE2 [20]. The ability of biogenic Mn dioxides produced by manganese-oxidizing bacteria to remove EE2 has also been evaluated [21]. These Mn oxide-based treatments display high efficiency for estrogen removal and provide additional technical approaches for EDC treatment.

In the natural environment, biogenic manganese oxidation, which is primarily accomplished by bacteria through enzymatic catalysis, represents a much faster pathway for Mn oxide mineralization [15]. Increasing evidence from a variety of marine and soil Mn^{2+}-oxidizing bacteria have indicated that oxidoreductase multicopper oxidase (MCO) oxidizes Mn^{2+} to Mn^{4+}, resulting in the formation of biogenic Mn oxides [22]. This oxidation process appears to occur on the cell surface [23,24]. Moreover, the ability of a range of naturally occurring or synthetic Mn oxides to promote the transformation of various organic pollutants has been verified [16,17], and MCO on the surface of bacteria was capable of catalyzing certain organic substrates [25,26]. Hence, a cell surface display strategy in which MCO is immobilized on the surface of bacterial cells is particularly attractive for the purpose of developing an MCO-mediated Mn oxide degradation system with increased reactivity.

Cell surface display technology enables rapid and goal-oriented reactions on the cell surface, thereby increasing reaction speed and minimizing toxicity of substances to living cells [27]. We previously developed two bacterial cell surface display systems for MCOs on *Bacillus thuringiensis* [28] and *Pseudomonas putida* [26] cells, and we demonstrated the enzymatic activities of these systems as whole-cell catalysts. Spore coat protein A (CotA) from *Bacillus* also has MCO-like oxidoreductase activity [29] and Mn^{2+}-oxidizing activity [30], which are involved in the formation of biogenic Mn oxides [30]. Hence, in the current study, we engineered *Escherichia coli* cells to develop a biodegradation composite capable of completely degrading EDCs. The *cotA* gene from a Mn^{2+}-oxidizing bacterium, *Bacillus pumilus* A56, was expressed as a chimeric "*inaQ-N/cotA*" gene with the gene *inaQ-N* from *Pseudomonas syringae* to enable *E. coli* cells to project the fusion protein InaQ-N/CotA on the cell surface. Both laccase enzyme activity and Mn^{2+}-oxidizing activity were confirmed in the engineered *E. coli* cells, and these cells underwent prolonged Mn^{2+}-rich cultivation to form regular aggregates consisting of engineered *E. coli* cells surrounded by Mn oxides. The degradability induced by the composite for two representative EDCs, BPA and NP, was compared with that induced by Mn oxides or engineered *E. coli* cells alone. Intermediates of ^{13}C-labeled BPA and ^{13}C-labeled NP degradation were assayed, and the abundance of $^{13}CO_2$ from the degradation reactions was determined. The residual estrogenic activity of the degradation products was assayed using the model organism *Caenorhabditis elegans* as an indicator. The superoxide radical ion concentrations in BPA-degradation and NP-degradation were determined during the reaction with the aim of providing hints about the possible degradation mechanisms by our composite.

2. Materials and methods

2.1. Chemicals, bacterial and nematode strains, and culture conditions

Stable isotope ^{13}C-labeled BPA and NP were purchased from Cambridge Isotope Laboratories, Inc. (Tewksbury, MA, USA). All other chemicals were analytical grade. *E. coli* JM109 was used as the host cell for plasmid constructions and surface display experiments. Laboratory stock *B. pumilus* A56, which was isolated from Fe-Mn nodules, was used as the parent strain for the gene *cotA*. Synchronized fourth-stage (L4) larvae from *C. elegans* wild-type strain N2 (Bristol) were used for bioassays of the estrogen toxicity of the EDC degradation products.

For plasmid construction, protein expression and surface localization experiments using recombinant *E. coli*, the cells were grown at 30 °C in lysogeny broth (LB) medium [31] supplemented with ampicillin at a final concentration of 100 μg mL^{-1} when appropriate. For the Mn oxidation assays and biodegradation experiments, all strains were cultured at 30 °C in Lept medium [32] containing 20 mmol L^{-1} 4-(2-hydroxyethyl)-1-piperazineethanesulfonic acid (HEPES, pH 7.2), 1 mmol L^{-1} $MnCl_2$, and 100 μg mL^{-1} ampicillin. Cells were grown in LB or Lept medium until reaching an OD_{600} of 0.6 after which isopropyl-β-D-thiogalactoside (IPTG) was added at a final concentration of 0.1 mmol L^{-1} and were cultured for an additional 24–120 h to induce recombinant protein expression in transformed *E. coli* cells.

2.2. Plasmid construction and transformation

Bacterial plasmid DNA was prepared using a standard procedure [31]. The *cotA* gene was amplified via polymerase chain reaction (PCR) from the *B. pumilus* A56 genome using the primers F_{cot1}: 5′−GCGCTGCAGATGAACCTAGAAAATTTG−3′ (the *Pst*I site is underlined) and R_{cot}: 5′−CTAGAATTCCTAAATAATATCCATCGG−3′ (the *Eco*RI site is underlined). The amplified fragment was sequenced, digested with *Pst*I/*Eco*RI, and then ligated to the *Pst*I/*Eco*RI sites of the *E. coli* expression vector pTrcHis C (Invitrogen), thereby yielding the plasmid pMB499 (Fig. S1A). To construct the fusion gene *inaQ-N/cotA*, the gene *cotA* was amplified from the plasmid pMB499 with the primers F_{cot2}: 5′−GCGGGATCCATGAACCTAGAAAAATTTG−3′ (the *Bam*HI site is underlined) and R_{cot}: 5′−CTAGAATTCCTAAATAATATCCATCGG−3′ (the *Eco*RI site is underlined). The resulting fragment was digested with *Bam*HI and *Eco*RI and then inserted into the *Bgl*II/*Eco*RI sites of a previously constructed plasmid, pMB102 [33], to generate the plasmid pMB500

harboring *inaQ-N/cotA* under the control of the IPTG-inducible *E. coli* promoter P_{trc} (Fig. S1A). *E. coli* cells were transformed as previously described [31]. The recombinant *E. coli* strains harboring pMB499 and pMB500 were termed MB499 and MB500, respectively.

2.3. CotA expression and polyclonal cotA antiserum preparation

Recombinant *E. coli* MB499 expressed CotA after induction with 0.1 mmol L^{-1} IPTG for 5 h at 28 °C. The expressed CotA was separated by SDS-PAGE on 12.5% gels (Fig. S2A). The CotA protein band was excised and purified using a Ni-affinity chromatography kit (WSBH Chromat. Co., Beijing, China). The purified CotA was separated again by SDS-PAGE. The excised CotA band was then used to prepare a polyclonal CotA antiserum following previously described procedures [34].

2.4. Assays for surface localization of InaQ-N/CotA

E. coli MB500 cells were grown at 37 °C, and the expression of InaQ-N/CotA was induced with 0.1 mmol L^{-1} IPTG for 5 h at 28 °C. Cell suspensions were passed through a French cell press (Thermo, USA) at 5000 psi. The disrupted mixtures were then fractionated following previous procedures [35]. The InaQ-N/CotA fusion protein prepared from the whole cell fraction (WC), cytoplasmic fraction (CP), and outer membrane fraction (OM) of *E. coli* MB500 cells was analyzed by SDS-PAGE in 10% polyacrylamide gels. The proteins in the gels were then transferred onto Hybond polyvinylidene fluoride membranes (Amersham, USA). Western blot analysis of the cell fractions was then performed using the polyclonal CotA antiserum as the primary antibodies. Immunofluorescence microscopy examination and fluorescence-activated cell sorting (FACS) analysis of the intact *E. coli* MB500 cells were also performed following previously described procedures [26], with the exception that the polyclonal anti-CotA antiserum was used as the primary antibody. FACS measurements were recorded as the percentage of total CotA-labeled cells relative to the total Cy5 fluorescence.

2.5. Scanning electron microscopy (SEM)

E. coli MB500 cells were grown in Lept medium containing 1 mmol L^{-1} Mn^{2+} for 5 days. The suspensions were centrifuged, and the samples were prepared to be measured following previously described procedures [36] prior to SEM using a JSM-6390/LV scanning electron microscope (NTC, Japan).

2.6. Powder X-ray diffraction

Bacterial biogenic Mn oxides were extracted as previously described [37]. The extracted samples were then freeze-dried to obtain Mn oxide powders for X-ray diffraction (XRD) analysis (Bruker D8 Advance X-ray diffractometer). Samples were placed on low-background quartz plates and scanned over the range of $2\theta = 5-85^{\circ}$, and a LynxEye array detector and Ni filter plate were employed. The measurements were performed under the following conditions: Cu Kα ($\lambda = 0.15418$ nm); tube voltage = 40 kV; tube current = 40 mA; and step scan with a step size = 0.02° and scan speed = 10° min^{-1}.

2.7. Degradation experiments

For the EDC degradation experiments, three different matrices with degradation activity were prepared. *E. coli* MB500 cells were incubated in Lept medium containing 1 mmol L^{-1} Mn^{2+} for 5 days. The final culture was pelleted by centrifugation at 10,000 rpm for 5 min, and the pellet was washed three times with phosphate-buffered saline (PBS) (pH 7.0). The cell pellet was examined using SEM and XRD. This mixture was a composite and designated the "MB-MN" matrix. A portion of the MB-MN was broken using a French pressure cell at 15,000 *psi* six times to disrupt the bacterial cells. The resultant mixture was designated matrix "MN". For comparison, the MB500 culture that was collected from Mn^{2+}-free medium was designated "MB".

The degradation reaction mixture consisted of BPA or NP at an initial concentration of 2 ppm and an appropriate amount of the degradation matrix with either Mn^{2+} oxide activity equivalent to 65 ppm of MnO_2 (MB-MN and MN) or whole-cell laccase activity equivalent to 800 U mL^{-1} of (MB-MN and MB) in 0.1 M sodium acetate buffer (pH 3.0). The reactions were performed in the dark. The EDC content of the reaction mixture was measured during the course of the reaction. The EDC relative removal value of the different matrices was calculated using the following formula:

$$\text{Relative removal value } (\%) = \frac{C_i - C_f}{C_i} \times 100 \quad (1)$$

where C_i denotes the initial EDC content, and C_f denotes the final EDC content. All experiments were performed at least in triplicate.

After the degradation reactions, the materials were collected from the reaction mixture by centrifugation (16,000 × g for 30 min), resuspended in an equal volume of 0.1 mol L^{-1} sodium acetate buffer, and shaken at 150 rpm for 24 h at 25 °C to determine the potential adsorption of EDCs by the three matrices. The suspensions were then centrifuged at 16,000 × g for 30 min. The contents of the EDCs in the supernatant fluids were measured following the procedures described above. The relative adsorption value of EDCs by the materials was calculated using the following formula:

$$\text{Relative adsorption value } (\%) = \frac{C_d}{C_i - C_f} \times 100 \quad (2)$$

where C_d, C_i and C_f denote the adsorption content, the initial content and the final content of EDCs, respectively.

2.8. Analytical assays

A continuous biodegradation experiment was performed, as described by Liu et al. [25]. Cell density was measured at 600 nm with a UV/VIS spectrophotometer (DU800 Nucleic Acids/Protein Analyzer, Beckman Coulter). For the whole-cell CotA laccase activity assay, cells were harvested and diluted to a unit cell density (OD_{600} = 1.0) with a PBS buffer (pH 7.0). Whole-cell CotA laccase enzymatic activity was measured using 2,2′-azino-bis (3-ethyl-benzthiazoline-6-sulfonic acid (ABTS) (Amresco, Solon, USA) as the substrate at 25 °C, according to a previously described method [28]. One unit of enzyme activity was defined as the amount of enzyme required for the oxidation of 1 μmol L^{-1} of ABTS per minute. The Mn^{2+}-oxidizing activity was determined by a standard leukoberbelin blue (LBB) spectrophotometric assay as previously described [38]. The amount of MnO_2 produced (1 μmol L^{-1} MnO_2 corresponds to 0.4 μmol L^{-1} $KMnO_4$) was defined as the Mn^{2+}-oxidizing activity of the bacterial cells.

The content of BPA and NP was determined by high-performance liquid chromatography with a mass spectrometer (LC-MS) using a reversed-phase Waters ACQUITY BEH C-18 column (2.1 mm × 50 mm × 1.7 μm) on an Agilent 1200/6460 LC/QQQ system. Prior to their introduction into the column, the sample solutions were filtered through a 0.45-μm membrane filter and degassed. The BPA and NP contents were determined according to the procedures described by Sajiki and Yonekubo [39] and Loos et al. [40], respectively.

The degradation products of BPA and NP were analyzed using an Agilent 7890A/5975C gas chromatography mass spectrometer (GC–MS) with an HP-5 MS fused-silica column (0.25 mm × 30 mm × 0.25 μm) based on previously described assay procedures for BPA [41] and NP [42].

The content of $^{13}CO_2$ from the reaction mixtures of ^{13}C-labeled BPA or ^{13}C-labeled NP degradations was detected using a MAT-271 isotope mass spectrometer (Finnigan Co., USA), following a procedure

described by Cao et al. [43]. Prior to the determination, 1 ppm each of ^{13}C-labeled BPA and ^{13}C-labeled NP was added to the degradation reaction container loaded with an appropriate amount of MB-MN, as described above. The container was sealed with wax immediately and was incubated at 30 °C while shaking at 150 rpm for 24 h.

The superoxide radical ion concentrations of BPA-degradation and NP-degradation were determined during the reaction time-course of 24 h following a method that was described previously [44].

2.9. Bioassays of degradation product estrogen toxicity

C. elegans was used as the model organism used to evaluate the estrogen toxicity of the EDC degradation products in eukaryotes. A multiple-generation toxicity bioassay was performed as described by Tominage et al. [45]. In brief, L4 larvae were transferred to NGM plates containing the BPA and NP degradation products. Similar procedures were performed to allow *C. elegans* to reproduce for more than five generations. The numbers of worms and eggs on the plates were counted from the fourth generation under a dissecting microscope at a fixed time every day to determine the sublethal toxicity (fecundity and reproduction) of the degradation products.

2.10. Continuous biodegradation experiments

For experiments involving three consecutive rounds of biodegradation, the biodegradation activity of MB-MN was tested at pH 3.0 and 25 °C. After the first-round reaction, the cells were harvested by centrifugation and used directly for the second-round and third-round reactions under similar conditions. The supernatant was removed by centrifugation after the second- and third-round reactions, and 100 mL Lept medium containing 1 mmol L^{-1} $MnCl_2$ was added to the flasks to allow the growth of residual cells at 30 °C and 200 rpm for 4 h. This procedure was not conducted under strict aseptic conditions. A subsequent fourth-round degradation reaction was performed under the same reaction conditions after the removal of the medium via centrifugation. The degradation rate in each round was determined.

2.11. Database search

The *cotA* sequence was characterized by conducting BLASTN and BLASTP searches on the GenBank nucleotide and amino acid (aa) sequence database using the National Center for Biotechnology Information (NCBI) server (http://blast.ncbi.nlm.nih.gov/Blast.cgi). The conserved domain architectures of CotA were analyzed using the NCBI online tool, “Conserved Domain Search” (http://www.ncbi.nlm.nih.gov/Structure/cdd/wrpsb.cgi).

2.12. Statistical analysis

Statistical analysis was performed using SPSS (Statistical Package for the Social Sciences) 13.0 statistical software. All data presented are the averages of at least three biological replicates. Statistical significance was defined as $P < 0.05$.

3. Results

3.1. Construction of the CotA surface-projecting system and characterization of CotA expression

The CotA-encoding gene was amplified by PCR from the genome of *B. pumilus* A56. Sequence analysis and alignment of the nucleotide sequence of *cotA* using the online BLASTN tool suggest that this 1530 bp gene (GenBank accession no. JQ035528.1) is a *Bacillus* spore coat protein CotA gene that shares 88% sequence identity with the *P. pumilus* SAFR-032 *cotA* gene (GenBank accession no. CP000813.1). The *cotA* gene encodes a 509 aa protein with a deduced molecular mass of 58.6 kDa and an isoelectric point of 6.12. The predicted full-length CotA protein contains four Cu^{2+}-binding motifs with residues that are conserved in similar motifs in other MCOs (Fig. S1B), suggesting that this CotA is an MCO.

Heterologous expression of CotA in recombinant *E. coli* MB499 was induced by IPTG. SDS-PAGE analysis of the expression products revealed a band (Fig. S2A, lane 1, indicated by the red arrow) that corresponded to the expected molecular mass for CotA (58.5 kDa) but was not present in the JM109 profile (the recipient strain). This band therefore corresponded to CotA.

A previously characterized functional cell surface display system in *E. coli* [33] was used for the surface projection of CotA to develop a system for displaying catalytic CotA on the surface of *E. coli*. The anchor gene *inaQ-N* was fused with *cotA* to create the chimeric *inaQ-N/cotA* in a single encoding frame (Fig. S1A). The expression and surface localization of InaQ-N/CotA in transformed *E. coli* MB500 cells were analyzed by Western blot, immunofluorescence microscopy and flow cytometry assays (Figs. S2B–D). The Western blot profile indicated that InaQ-N/CotA was present in the OM fraction (Fig. S2B, lane OM) of the transformed cells because the OM-complex fraction exhibited a protein band corresponding to those present in the WC and CP fractions (Fig. S2B, lanes WC and CP). Immunofluorescence microscopy revealed clear Cy5 fluorescence on the cell surface of MB500 (Fig. S2C), thereby verifying the surface localization of CotA because the externally added macromolecular Cy5-tagged antiserum cannot penetrate the outer membrane. This result is consistent with the results of the FACS assay, in which pronounced Cy5 fluorescence intensity was observed in intact MB500 cells (Fig. S2D). In contrast, only limited Cy5 fluorescence was observed in the negative control cells. Thus, these analyses confirmed the successful projection of the CotA protein onto the surface of *E. coli* MB500 cells.

The whole-cell laccase activity and Mn^{2+}-oxidizing activity of MB500 cells were monitored over the course of a 144 h culture in Lept medium containing 1 mmol L^{-1} Mn^{2+} (Fig. 1A). Upon induction of protein expression by IPTG at 5 h, the whole-cell laccase activity of the MB500 cells increased to a maximum value of 26.4 U mL^{-1} at 6 h (the highest activity of MB500 cells is higher than those the other two surface-displayed laccases, MCO266 [24] and WlacD [28]), reduced to an activity of approximately 20.0 U mL^{-1} between 6 and 48 h, and exhibited an activity of 19.1 U mL^{-1} at 144 h. Mn^{2+}-oxidizing activity was detectable within 24 h and then exhibited a steadily increasing pattern from 24 − 120 h. Interestingly, during the later growth phase, the MB cells formed regular microspherical aggregates. SEM (Fig. 1B) revealed that these aggregates varied in diameter from approximately 10 μm to 20 μm; attached and embedded bacteria were observed around the aggregates. Notably, the pH of the MB500 culture suspension remained lower than 8.0 during the entire culture period, which prevented the abiotic oxidation of Mn^{2+} because the reaction occurs preferentially at pH > 8.0 [46]. Moreover, although anaerobic conditions are favorable for the formation of some Mn compounds, such as rhodochrosite ($MnCO_3$) [47] or MnS [48], the use of Lept medium, which lacks CO_3^{2-}, should not favor this formation because $MnCO_3$ has been reported to form idiomorphically at pH > 8, $CO_3^{2-} > 4.4 \times 10^{-3}$ mmol L^{-1} and Eh < 418 mV [48]. On the other hand, we have previously confirmed that in a reaction system with only *E. coli* JM109 cells and organic substrates, soluble Mn^{2+} failed to be oxidized to Mn^{4+} in the absence of MCO [24]. Therefore, the observed aggregates were most likely formed by CotA-catalyzed biogenic Mn oxidation and not by an abiotic process.

3.2. XRD analysis of Mn oxides

XRD assays were performed to verify the types of Mn oxides in the microspherical aggregates. The XRD pattern of the aggregate samples showed six characteristic peaks at 4.22 Å, 3.34 Å, 2.46 Å, 2.37 Å, 2.18 Å and 1.70 Å corresponding to MnO_2 (JCPDS 00–042-1316), four

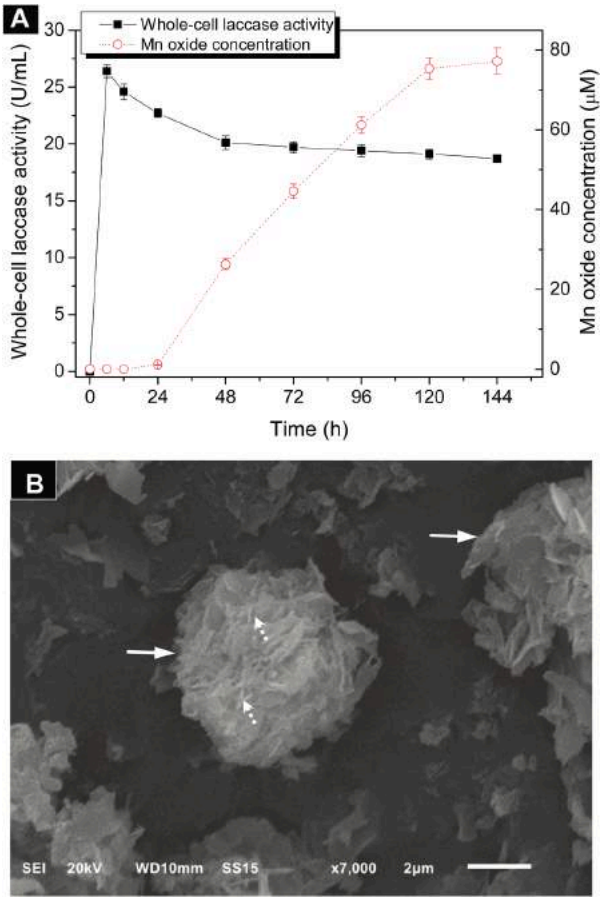

Fig. 1. Time course of the whole-cell CotA laccase activity and Mn^{2+}-oxidizing activity of the engineered *E. coli* MB500 cells (A) and a representative SEM micrograph of the aggregates formed in MB500 cultures (B). In (A), the cells were grown in Lept medium for 144 h, and activity measurements were performed using a unit cell density (OD_{600} = 1.0) at 6 h and 12 h and then every 24 h. In (B), the solid arrows indicate the aggregates, and the dotted arrows indicate the MB500 cells attached to the aggregates.

characteristic peaks at 4.07 Å, 2.55 Å, 2.34 Å and 1.66 Å corresponding to MnO_2 (JCPDS 00-039-0375), and three characteristic peaks at 4.03 Å, 2.43 Å and 1.65 Å corresponding to MnO_2 (JCPDS 00-044-0142) (Fig. 2). These peaks are consistent with the main characteristic peaks of natural ramsdellites. Therefore, these results confirmed that the microspherical aggregates formed by MB500 were mainly composed of ramsdellites (MnO_2).

3.3. Evaluation of the EDC removal efficiencies of the matrices

Two representative EDCs, BPA and NP, were selected as degradation substrates to evaluate the removal efficiency of the three matrices. As shown in Fig. 3, under the experimental conditions (i.e., pH 3.0, 25 °C, 2 ppm each EDC, and 60 min reaction time), all three matrices were capable of rapidly removing BPA and NP in 60 min; however, the activity of MB-MN was greater than those of MN or MB alone, which reflects an associated action of MB500 cells and Mn oxides in this matrix that led to increased EDC removal.

3.4. Effects of pH, temperature, initial EDC concentration and heavy metals on removal efficiency

Fig. S3 shows that a relatively low pH favored BPA and NP removal because all three matrices exhibited the highest relative removal value at pH 3.0, but the effectiveness lasted across pH 3–7, especially for MB-MN. Fig. S4 shows the diverse effects of temperatures ranging from 15 °C to 55 °C on BPA/NP removal by the three matrices. The BPA/NP removal activity of MB-MN was greater than that of MB and MN throughout the measured temperature range and the activity had two relative peak values at 25 °C and 55 °C. Based on these results, in the subsequent treatments, the reaction parameters were set to the values of the optimal pH (pH 3.0) and temperature (25 °C for MB-MN and MB, 55 °C for MN) with a reaction time of 60 min.

Fig. S5 shows that the three matrices have good removal effects on EDCs at different initial concentrations. The absolute amount of EDCs eliminated by the three matrices may not be comparable because the matrix concentration cannot be normalized to a unit activity level; however, it is apparent that these matrices are capable of eliminating a very low level of EDCs (0.1 ppm).

All metal ions (i.e., Cu^{2+}, Zn^{2+}, Mn^{2+}, Mg^{2+}, Fe^{3+}, and Al^{3+}) inhibited the BPA/NP relative removal values of all three matrices at 1 mmol L^{-1} in 20 min (Fig. S6A and B), which is consistent with the results of previous studies on abiotic Mn oxides [18] and biogenic Mn oxides [21]. However, at a concentration of 0.1 mmol L^{-1}, diverse effects were observed for different metals (Figs. S6C and D). Cu^{2+}

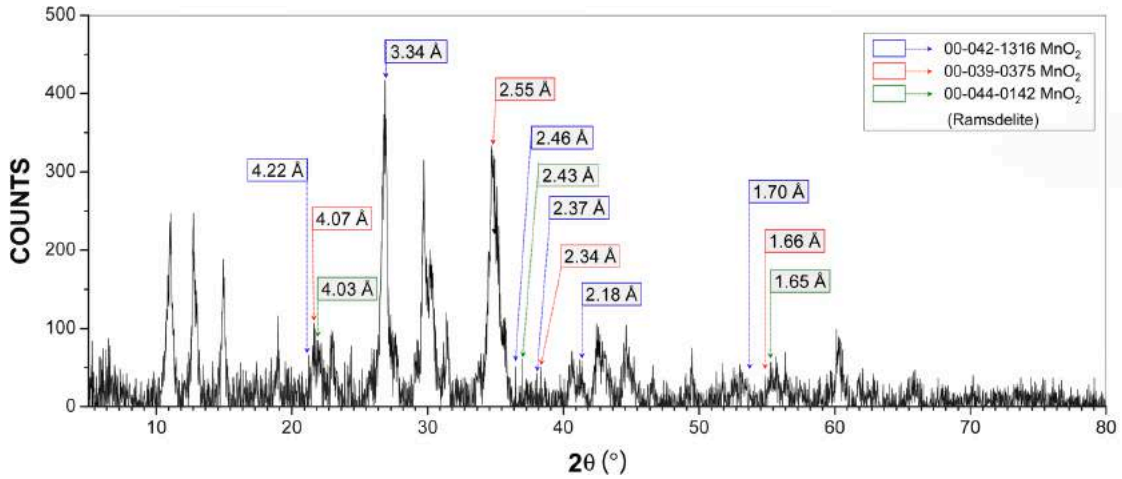

Fig. 2. XRD patterns of biogenic Mn oxides of the microspherical aggregates formed by MB500 cells.

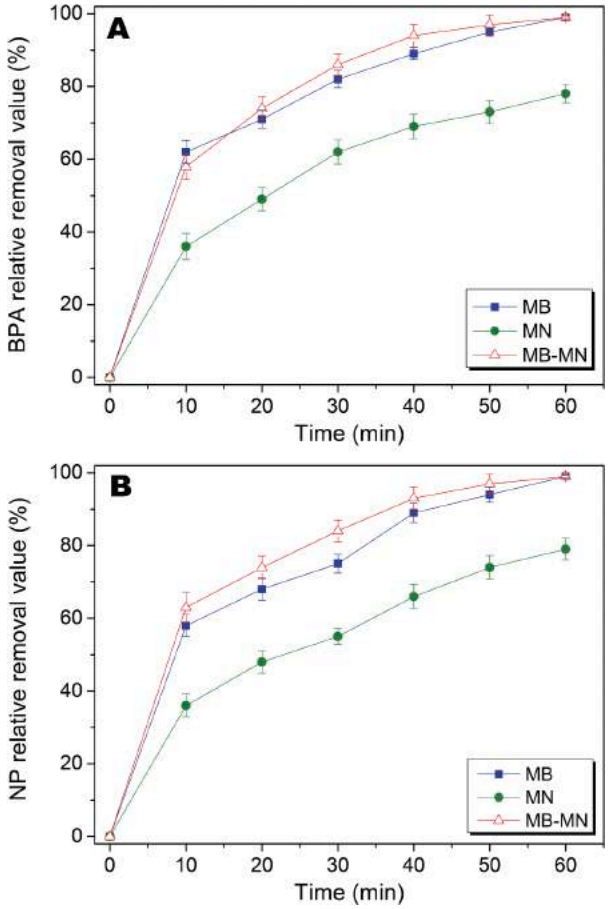

Fig. 3. Relative removal values of BPA (A) and NP (B) by MB, MN and MB-MN. The experimental were operation under pH 3.0, 25 °C, 2 ppm initial concentration of each EDC, and 60 min of reaction time.

significantly increased the activities of MB-MN and MB, whereas the other metals had no noticeable effect on any of the three matrices. A low concentration of Cu^{2+} has been reported to enhance MCO enzymatic activity [28], which is consistent with the enhancement of MB and MB-MN activity but not MN activity by Cu^{2+}. In contrast with previous studies that demonstrated a substantial decrease in laccase activity in the presence of various metal ions [49], the laccase activity of CotA was not significantly affected by these metal ions, suggesting that the cell platform on which CotA was surface-immobilized facilitates the retention of activity in the presence of these metal ions.

3.5. Detection of EDC adsorption by the matrices

The adsorbed and residual BPA and NP contents were determined from comparably normalized 24 h reactions in solutions containing each EDC at an initial concentration of 1 ppm. EDC adsorption by MB and MB-MN was very limited, with percentages of total BPA or NP adsorption of less than 8% (by MB) and 3% (by MB-MN), while in contrast, MN adsorbed approximately 64% of the total BPA and 69% of the total NP (Fig. 4). Interestingly, all matrices nearly completely eliminated BPA and NP; the highest residual EDCs were less than 2% for MB, 4% for MN and were undetectable for MB-MN. These results demonstrate that the removal of the EDCs by both MB and MB-MN was due to direct biodegradation rather than adsorption, whereas the removal of the EDCs by MN was mainly due to adsorption. However, the low level of residual EDCs in MN indicated that this matrix could also

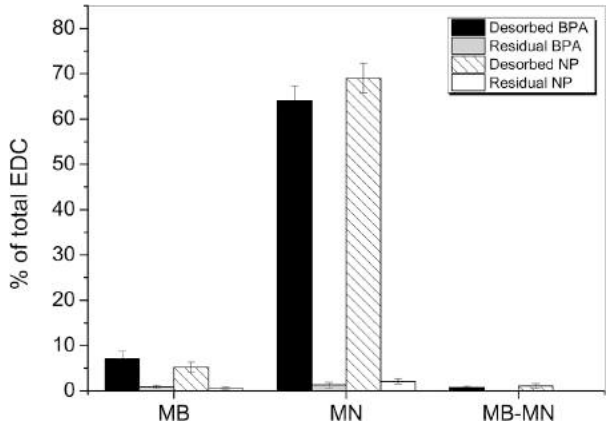

Fig. 4. Measurement of adsorbed or residual BPA and NP after treatment with MB, MN and MB-MN. % of total EDC, the percentage of desorbed or residual BPA and NP of their initial concentrations.

degrade EDCs.

3.6. Degradation product analysis

GC–MS assays were performed to identify the degraded products of ^{13}C-labeled BPA and ^{13}C-labeled NP by the three matrices. After 24 h of reaction time, only a few peaks above the baseline were visible in any of the supernatant fluids (Fig. S7) with amounts equivalent to approximately 1–5% of the BPA/NP loading and nearly under the detection limit of the GC–MS system, which indicates that these EDCs were nearly completely degraded or adsorbed by MB-MN or MN. However, when the reaction mixtures with different reaction times were subjected to GC–MS assays, as shown in Table 1, a total of 7 intermediates from BPA-degraded products by MB-MN and a total of 10 intermediates from NP-degraded products by MB-MN (4 intermediates), MB (3 intermediates), and MB-MN/MB (3 intermediates) were identified. Among the identified intermediates, 2,4-bis(1,1-dimethylethyl) phenol has been identified as an intermediate from the BPA-degraded product of chemically synthesized Mn oxides [50], 1,2-dimethoxy-benzene is structurally similar to that of BPA-degraded products by a recombinant laccase [51], and 2-methyl-4-(1,1,3,3-tetramethylbutyl)-phenol and 4-(1,1-dimethylpropyl)-phenol from the NP-degraded products are analogues to NP isomers [52]. Due to the rapid degradation of EDCs by MB-MN and the late sampling time, the identified products in the early stage of degradation reaction are less. Therefore, some other intermediates might still remain unidentified. Nevertheless, the occurrence of these intermediates verified the biodegradation by MB-MN or MB as a result of the joint processes of cellular enzymatic catalysis and cooxidation reactions of the catalytic CotA on the cell surface and Mn oxides.

The 24 h degradation products of ^{13}C-labeled BPA and ^{13}C-labeled NP by MB-MN were further analyzed for the occurrence and concentration of $^{13}CO_2$. As expected, $^{13}CO_2$ was detectable in the degraded products of both ^{13}C-labeled BPA and ^{13}C-labeled NP. In contrast with the background level of $^{13}CO_2$ in the control sample, approximately 80% equivalent ^{13}C-labeled BPA and approximately 84% equivalent ^{13}C-labeled NP were converted to $^{13}CO_2$ (Fig. 5).

3.7. Detection of the superoxide radical contents

The total superoxide radical (SR) contents of the BPA-degradation and NP-degradation reaction mixtures were monitored during the 24 h reaction period with the three matrices. Relatively high initial SR concentrations were recorded in the MB-MN and MN samples (Fig. 6A and B), which was consistent with some previous investigations that

Table 1
GS-MS identified intermediates of BPA- and NP-degradation by MB-MN, MB or MB-MN.

Degraded product	Mw	Degraded by	EI characteristic ions (*m/z*)	Retention time (min)
Degraded intermediates of BPA:				
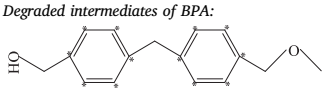	254	MB-MN	254, 223, 191, 177, 148, 113, 85	53.868
[4-(4-Methoxymethylbenzyl)phenyl]methanol				
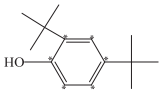	212	MB-MN	41, 57, 169, 196, 212	24.943
2,4-bis(1,1-dimethylethyl) phenol				
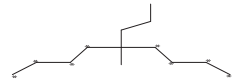	192	MB-MN	146, 131, 117, 103, 89, 75, 61,46	16.324
5-methyl-5-propyl-nonane				
	176	MB-MN	176, 133, 119, 103, 88, 73, 57, 43	7.315
3,7-dimethyl-decane				
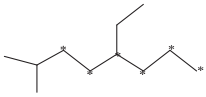	162	MB-MN	162, 133, 119, 103,89,73, 59, 43	17.741
5-ethyl-2-methyl-octane				
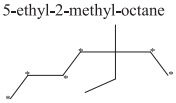	147	MB-MN	132, 117, 89, 75, 58, 44	16.020
3-ethyl-3-methylhepthne				
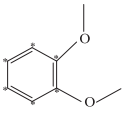	144	MB-MN	144, 129, 101, 83	18.281
1,2-dimethoxy-benzene				
Degraded intermediates of NP:				
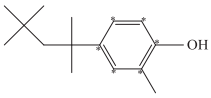	226	MB-MN/MB [a)]	226, 155, 127, 57, 41	16.771
2-methyl-4-(1,1,3,3-tetramethyl butyl)-phenol				
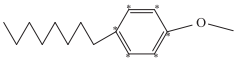	226	MB	226, 155, 127, 91, 77, 57, 41	15.643
1-methoxy-4-octyl-benzene				
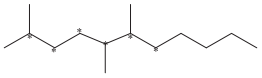	184	MB	156, 132, 117, 101, 87,72, 58, 43	7.380
2,5,6-trimethyl-decane				
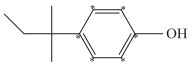	170	MB	170, 155, 142, 125, 113, 101, 77, 55, 41	14.527
4-(1,1-dimethylpropyl)-phenol				
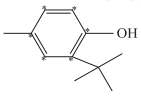	170	MB-MN	170, 155, 140, 127, 111, 97, 83	15.554
2-(1,1-dimethylethyl)-4-methyl-phenol				

(*continued on next page*)

Table 1 (*continued*)

Degraded product	Mw	Degraded by	EI characteristic ions (*m/z*)	Retention time (min)
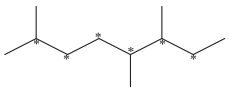	162	MB-MN	162, 103, 88, 74	6.753
2,5,6-trimethyl-octane 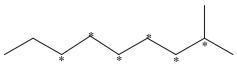	162	MB-MN	148, 103, 89, 74, 59, 44	6.817
2-methyl-nonane 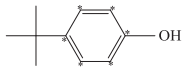	156	MB-MN	156, 141, 125, 113, 101, 83, 41	15.674
p-tert-butyl-phenol 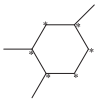	132	MB-MN	132, 117, 72, 58, 41	6.701
1,2,4-trimethyl-cyclohexane 	132	MB-MN/MB	132, 117, 72, 58, 41	6.522
1,1,3-trimethyl-cyclohexane				

a) Occurs in both MB-MN and MB degradation reactions.
b) *, C atom with ^{13}C stable isotope.

revealed the occurrence of large amounts of SR along with the process of Mn oxide formation [41]. Interestingly, following the degradation reaction processes, the MN- and MB-produced SRs from either the BPA-degradation (Fig. 6A) or NP-degradation reaction (Fig. 6B) sharply decreased, whereas MB-MN-produced SRs maintained relatively high levels in both the BPA- and NP-degradation reactions throughout the time period.

3.8. Bioassays of estrogenic activity

The incomplete degradation or simple adsorption of EDCs may lead to new or transferred hazards to environmental organisms and humans due to estrogen toxicity. The model eukaryote *C. elegans* was used to evaluate the effect of the degradation products and the postreaction matrices on nematode fecundity to investigate the estrogenic activity of the products of degradation by the three matrices. Pure BPA and NP alone exhibited apparent estrogenic activities, whereas both the degradation products and postreaction matrix of MB-MN exhibited no such activities (Fig. 7A and B). In contrast, the degradation products by MB and the postreaction MB cells exhibited comparably higher residual estrogenic activities. No residual estrogenic activity is observed for the MN degradation products; however, the postreaction MN matrix exhibited activity. These findings are consistent with the results presented in Fig. 4, in which significant adsorption activities were observed in all postreaction MN matrices.

3.9. Repeated EDC biodegradation performance of MB-MN

Three consecutive rounds of biodegradation by MB-MN were performed to evaluate the repeatability of BPA and NP biodegradation. MB-MN induced high degradation rates of two EDCs, with degradation rates in excess of 98%, 91%, and 86% in the consecutive first-, second- and third-round degradations, respectively (Fig. 8). Furthermore, the degradation activity was at least 94% when a simple culturing process was used. These results demonstrate that the MB-MN matrix has high performance in terms of repeatability and regeneration.

4. Discussion

The data presented in this study suggests that the dynamic oxidation system comprising a composite of biogenic Mn oxides and engineered bacterial cells with surface-immobilized CotA exhibited strong oxidative capacities for degrading the tested EDCs. The engineered cells oxidatively degraded the EDCs to specific intermediates depending on the activity of the surface-displayed CotA, which overcame the mass transfer limitations or passive diffusion of the substrates to increase degradation efficiency. The Mn oxides played several roles in the

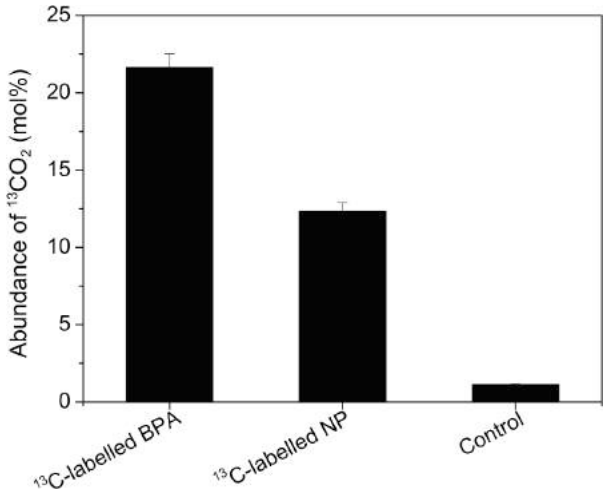

Fig. 5. Abundance of $^{13}CO_2$ from ^{13}C-labeled BPA and ^{13}C-labeled NP degraded products by MB-MN. Each initial 1 ppm ^{13}C-labeled BPA or ^{13}C-labeled NP was degraded by MB-MN for 2 h in a gas seal device. The collected $^{13}CO_2$ was detected using a MAT-271 isotope mass spectrometer (Finnigan Co., USA). Control: the free air sample from the device.

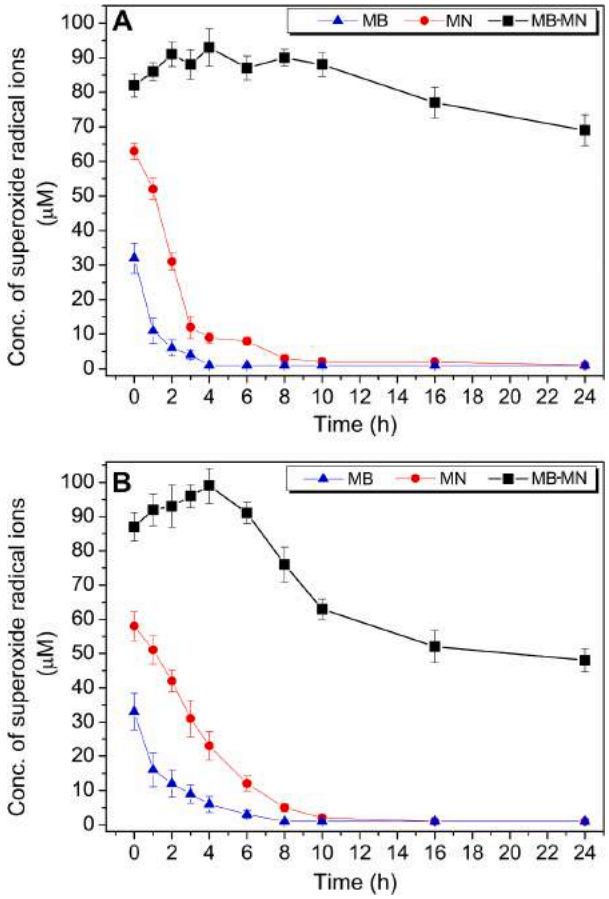

Fig. 6. Time course of the superoxide radical ion concentrations of BPA- and NP-degradation reaction solutions. Each initial 1 ppm BPA (A) or 1 ppm NP (B) was used as the reaction substrate.

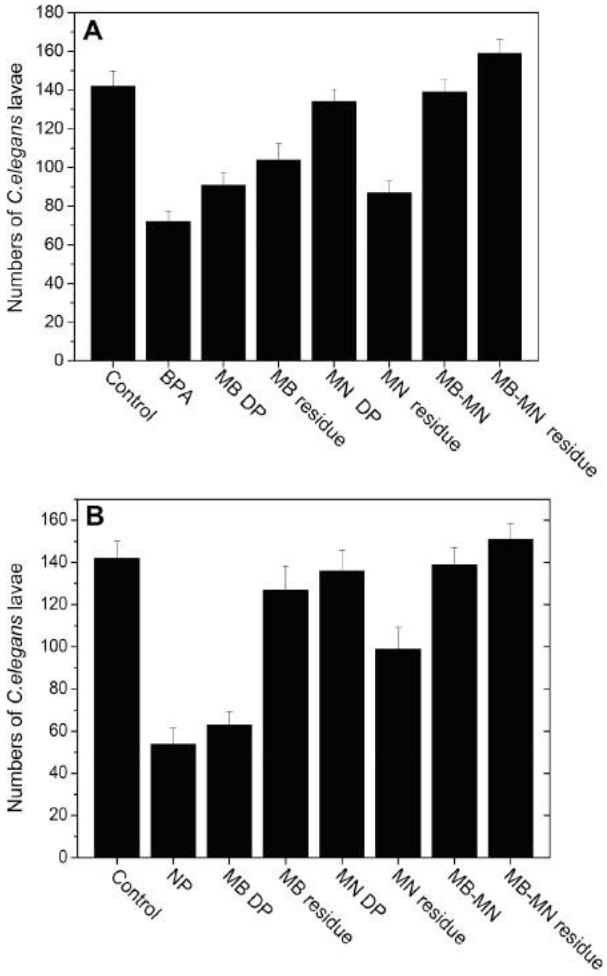

Fig. 7. Effects of EDC degradation products on the fecundity of *C. elegans*. (A) and (B), *C. elegans* numbers after treatment with the products of BPA and NP degradation, respectively. DP is the degraded product.

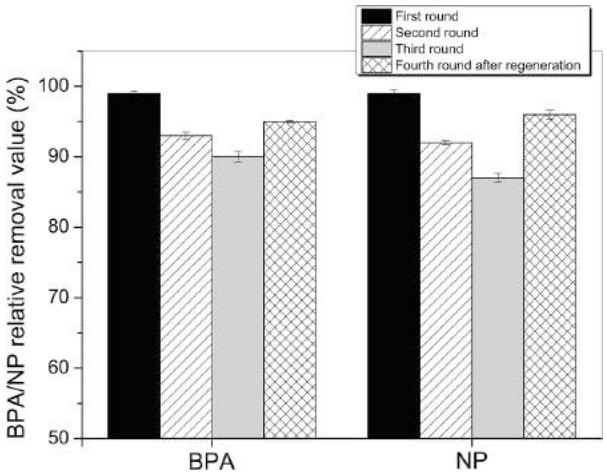

Fig. 8. Continuous degradation of BPA and NP by MB, MN and MB-MN.

reaction, including degrading the EDCs through SR-mediated oxidation, rapidly adsorbing the EDCs, providing favorable catalytic micro-environments, converting EDCs to easily degraded isomers [53], and acting as stable platforms to facilitate the oxidative reactions of both the engineered bacterial cells and the Mn oxides themselves. In addition, the MN matrix adsorbed the engineered cells during aggregate formation to embed or attach the cells (Fig. 1B) and free CotA proteins that were released from cells lysed during cell culture, which led to Mn oxidation and aggregate formation. Thus, the composite MB-MN likely possessed different active constituents with oxidative potential: the engineered cells embedded or attached to the aggregates, the biogenic Mn oxides, the free CotA proteins, and the various SRIs, as identified above (Fig. 6). While MB alone exhibited only incomplete degradation of the EDCs and MN alone exhibited adsorption activity rather than direct degradation during the reaction course, the composite MB-MN associatively combined the degradation capacities of both MB and MN to form an integrated metabolic pathway of EDCs.

Several previous investigations have manifested higher degradation levels of BPA, NP or other organic matters under acidic conditions by all four crystal forms of MnO_2 (i.e., α-, β-, γ-, and δ-MnO_2) that were chemically synthesized (Table S1). Among these Mn oxides, δ-MnO_2 exhibited the highest degradation efficiencies, which were attributed to its high oxidation degree, large specific surface area and abundant surface holes [18]. Certain biogenic Mn oxides have been characterized as hexagonal symmetrical weak crystal layered minerals, which are closest to chemically synthesized δ-MnO_2 and birnessite [54]. These biogenic Mn oxides typically exhibit additional characteristics, such as small particle sizes, unordered accumulation along the C axes, high valences, and several vacancies in their octahedral structures [55].

Similarly, the MB-MN developed in this study was an amorphous, weakly crystalline mixture consisting of various Mn oxides (Mn^{4+}, Mn^{3+}, and Mn^{2+}) that mainly consisted of ramsdellites mixing with other oxides such as birnessite, and crystal forms that mainly consisted of γ-MnO_2 and δ-MnO_2 with abundant octahedral vacancies, which are presumed to be conducive to the adsorption of organic matters [56] and the capture of SRs [57]. Moreover, the crystallinity of this weakly crystalline Mn oxide can be enhanced by aging or ion exchange and is likely converted to a triclinic birnessite or a todorokite analog [58]. Thus, these structural features confer MB-MN significant potential as an oxidizer and a sorbent, which enables a coordinated and effective degradation of BPA and NP.

On the other hand, similarly to other *E. coli* strains, the engineered MB harbored other oxidoreductases in addition to the surface-displayed laccase CotA, such as superoxide dismutase, and peroxidase. As shown in Fig. S2, MB alone exhibited a degradation effect on BAP and NP to some extent, which might be attributed to the joint degradation of these enzymes. We presume that the primary roles of MB cells include the following aspects: (i) serving as an oxidizer for the formation of Mn oxides and for oxidizing the organic substrates; (ii) serving as a nucleating center for the formation of Mn oxide aggregates as confirmed in a previous Mn^{2+}-oxidizing bacterium with surface-displayed MCO [24]; and (iii) serving as an initial donor of SRs because SRs are likely generated during the growth of MB cells and during the oxidation process of CotA [59]. Interestingly, several previous investigations have confirmed that certain abiotic Mn oxides had only limited degradation efficiencies on organic substrates without an oxidizing agent, such as peroxymonosulfate, peroxydisulfate, and hydrogen peroxide [60–62], which strongly contrasts the significant degradation efficiencies of MB-MN without such oxidizing agents, thereby indicating the significance of MB during the degradation process of MB-MN. It is noteworthy that the cellular enzymes of MB could also exert a suppressing effect on the radicals. The relatively low detectable level of SRs in MB (Fig. 6) is presumable to be an elimination consequence of certain cellular enzymes including superoxide dismutase, peroxidase, etc. [63]; however, the fate of the SRs in MB-MN is different because the SRs can be captured by Mn oxides following generation, which then serve as functional degraders towards the BPA and NP. Thus, under the associated degradation of MB and MN, BPA and NP were completely degraded. Although a relatively prolonged culture process is required for the formation of MB-MN, the significant degradation capability enabling mineralization of BPA and NP indicated one of its intrinsic advantages over other abiotic Mn oxides (Table S1).

The high level of SRs in the MB-MN reaction mixtures (Fig. 6) suggests a correlation between the SRs and the BPA-degradation and NP-degradation. Many previous investigations have demonstrated that active oxygen radicals were able to degrade or mineralize various refractory organic pollutants through advanced oxidation processes (AOPs) (for reviews, see [64,65]). In these AOPs, photochemical and/or electronic radiation or catalysts and those combined with certain oxidants are used to produce highly active oxygen radicals; these radicals lead to various reactions (*e.g.,* adduction, substitution, electron transfer, and bond breaking) with target compounds and oxidatively degrade these toxic compounds into less toxic or nontoxic substances, or even directly convert them into CO_2 and H_2O [65]. Mn oxides are rich in the natural environment and have been shown to be promising as effective heterogeneous catalysts to activate oxidants [66]. In the process of aromatic substrate degradation by Mn oxides, SRs can be relatively stable through the interaction between the oxides and the aromatic substrates after being trapped by the vacancies in the Mn oxides. Thus, these SRs can directly attack the π-electron clouds of the benzene rings, can oxidize polycyclic aromatic hydrocarbons to degraded compounds, such as benzoic acid, and then can decompose them to small molecular compounds, such as formic acid and acetic acid [57]. Therefore, SRs produced by MB-MN could be the major reactive species degrading BPA or NP, especially during the initial oxidation processes, which leads to benzene ring cleavages and other degradation reactions.

Hence, based on the compositional analysis of the intermediates (Table 1), we propose the following stepwise pathways for degradation by the composite MB-MN, in which the BPA and NP are subjected to similar degradation processes. (1) Prior to degradation, the EDC molecules are adsorbed by the MN and accumulate on the surfaces and possibly on the shallower layers of the aggregates. The aggregates serve as platforms for the subsequent oxidative reactions. (2) Oxidative or enzymatic the degradation of BPA and NP into smaller MW intermediates is performed by SRs, surface-displayed CotA and select cellular enzymes. Multiple related reactions, such as methylation/demethylation, benzene ring cleavage, hydroxylation, hydrogenation, and alkyl degradation, are predicted to occur during the processes. In the case of BPA degradation (Fig. S8), we propose several possible degradation pathways. Two rings could be converted into a single ring and an alkyl chain, or two rings could be directly converted to an alkyl chain. However, in NP degradation (Fig. S9), the NP was converted following the reactions of benzenes to lower alkyl compounds by different routes. Certain SRs could play crucial roles in degrading BPA/NP into lower intermediates, especially in cleaving the benzene rings, an activity that has been shown in some other investigations [67,68]. (3) Finally, these lower alkyl compounds are ultimately converted to CO_2 and H_2O through joint oxidation by the engineered cells and the Mn oxides.

It is noteworthy that the as-prepared MB-MN composite had a favorable performance under acidic conditions but only limited degradation activity on organic substrates in alkaline solutions. However, acidic wastewater is widely present in a variety of industrial fields, such as ammunition manufacture, pharmacy, mining sites, steel manufacture, electroplating and phosphorous industries [69]. On the other hand, given the ability of laccase-like enzymes to degrade synthetic dyes and organic pollutants [25,26], as well as the ability of Mn oxides to degrade a variety of organic pollutants and remove heavy metals [16,17], the potential applications of this composite could extend to other fields, including industrial wastewater processing, heavy metal detoxification, and biotransformation of environmental pollutants.

5. Conclusions

The current study demonstrated for the first time the complete biodegradation of two representative EDCs, BPA and NP, using a composite composed of biogenetic Mn oxides and engineered bacterial cells with surface-immobilized CotA. Mn oxidation by the CotA laccase on the surface of the target cells led to the formation of microspherical aggregate composites. X-ray diffraction analysis confirmed that the aggregates were primarily composed of ramsdellite. Under optimized reaction conditions, the composite degraded the EDCs into the final product, CO_2, and thereby completely eliminated their estrogenic activities. Based on its repeatable, rapidly recoverable performance, adequate physical strength, and the requirement for only normal reaction conditions, the developed composite may be particularly valuable for the biotreatment of EDC-containing wastewaters in large-scale or continuous bioprocesses.

Acknowledgments

The authors are grateful to Dr. Changsong Zhao for his technical help with the XRD experiments and data analysis, Prof. Ming Sun for providing the *C. elegans* wild-type strain N2 (Bristol), and Dr. Donghai Peng for experimental guidance on the bioassays. This work was supported by grants from the National Natural Science Fundation of China (Grant Nos. 31770108 and 31570123) and was supported by the Fundamental Research Funds for the Central Universities of China (Program no. 2662015PY189) and a grant from the State Key Laboratory of Agricultural Microbiology, Huazhong Agricultural University, China (Grant No. AMLKF201706).

Appendix A. Supplementary data

Supplementary data to this article can be found online at https://doi.org/10.1016/j.cej.2019.01.062.

References

[1] H. Cabana, J.P. Jones, S.N. Agathos, Elimination of endocrine disrupting chemicals using white rot fungi and their lignin modifying enzymes: a review, Eng. Life Sci. 7 (2007) 429–456.
[2] H.A. Jeng, Exposure to endocrine disrupting chemicals and male reproductive health, Front. Public Health 2 (2014) 55.
[3] J. Knez, Endocrine-disrupting chemicals and male reproductive health, Reprod. Biomed. Online 26 (2013) 440–448.
[4] C. Casals-Casas, B. Desvergne, Endocrine disruptors: from endocrine to metabolic disruption, Annu. Rev. Physiol. 73 (2011) 135–162.
[5] C.E. Purdom, P.A. Hardiman, V.V.J. Bye, N.C. Eno, C.R. Tyler, J.P. Sumpter, Estrogenic effects of effluents from sewage treatment works, Chem. Ecol. 8 (1994) 275–285.
[6] C.L.S. Vilela, J.P. Bassin, R.S. Peixoto, Water contamination by endocrine disruptors: impacts, microbiological aspects and trends for environmental protection, Environ. Pollut. 235 (2018) 546–559.
[7] H.S. Chang, K.H. Choo, B. Lee, S.J. Choi, The methods of identification, analysis, and removal of endocrine disrupting compounds (EDCs) in water, J. Hazard. Mater. 172 (2009) 1–12.
[8] D.P. Mohapatra, S.K. Brar, R.D. Tyagi, R.Y. Surampalli, Physico-chemical pretreatment and biotransformation of wastewater and wastewater sludge-fate of bisphenol A, Chemosphere 78 (2010) 923–941.
[9] Q. Husain, S. Qayyum, Biological and enzymatic treatment of bisphenol A and other endocrine disrupting compounds: a review, Crit. Rev. Biotechnol. 33 (2013) 260–292.
[10] T. Fukuda, H. Uchida, Y. Takashima, T. Uwajima, T. Kawabata, M. Suzuki, Degradation of bisphenol A by purified laccase from *Trametes villosa*, Biochem. Biophys. Res. Commun. 284 (2001) 704–706.
[11] H. Kum, M.K. Kim, H.T. Choi, Degradation of endocrine disrupting chemicals by genetic transformants in *Irpex lacteus* with an inducible laccase gene of *Phlebia tremellosa*, Biodegradation 20 (2009) 673–678.
[12] H. Kum, S. Lee, S. Ryu, H.T. Choi, Degradation of endocrine disrupting chemicals by genetic transformants with two lignin degrading enzymes in *Phlebia tremellosa*, J. Microbiol. 49 (2011) 824–827.
[13] J.S. Sabirova, L.F. Cloetens, L. Vanhaecke, I. Forrez, W. Verstraete, N. Boon, Manganese-oxidizing bacteria mediate the degradation of 17alpha-ethinylestradiol, Microb. Biotechnol. 1 (2008) 507–512.
[14] T. Cajthaml, Z. Kresinova, K. Svobodova, M. Moder, Biodegradation of endocrine-disrupting compounds and suppression of estrogenic activity by ligninolytic fungi, Chemosphere 75 (2009) 745–750.
[15] B.M. Tebo, J.R. Bargar, B.G. Clement, G.J. Dick, K.J. Murray, D. Parker, R. Verity, S.M. Webb, Biogenic manganese oxides: properties and mechanisms of formation, Annu. Rev. Earth. Plant Sci. 32 (2004) 287–328.
[16] M.M. Najafpour, G. Renger, M. Holynska, A.N. Moghaddam, E.M. Aro, R. Carpentier, H. Nishihara, J.J. Eaton-Rye, J.R. Shen, S.I. Allakhverdiev, Manganese compounds as water-oxidizing catalysts: from the natural water-oxidizing complex to nanosized manganese oxide structures, Chem. Rev. 116 (2016) 2886–2936.
[17] H. Xu, N. Yan, Z. Qu, W. Liu, J. Mei, W. Huang, S. Zhao, Gaseous heterogeneous catalytic reactions over Mn-based oxides for environmental applications: a critical review, Environ. Sci. Technol. 51 (2017) 8879–8892.
[18] K. Lin, W. Liu, J. Gant, Oxidative removal of bisphenol A by manganese dioxide: efficacy, products, and pathways, Environ. Sci. Technol. 43 (2009) 3860–3864.
[19] L.Y. Jiang, J.M. Chen, R.Y. Zhu, C. Huang, H. Ji, Degradation kinetics and estrogenic activity of 17β-estradiol removal by aqueous manganese dioxide, J. Environ. Sci. Health A Tox. Hazard. Subst. Environ. Eng. 45 (2010) 938–945.
[20] L. Xu, C. Xu, M. Zhao, Y. Qiu, G.D. Sheng, Oxidative removal of aqueous steroid estrogens by manganese oxides, Water Res. 42 (2008) 5038–5044.
[21] D.-G. Kim, S. Jiang, K. Jeong, S.-O. Ko, Removal of 17α-ethinylestradiol by biogenic manganese oxides produced by the *Pseudomonas putida* strain MnB1, Water Air Soil Pollut. 223 (2012) 837–846.
[22] J.P. Ridge, M. Lin, E.I. Larsen, M. Fegan, A.G. McEwan, L.I. Sly, A multicopper oxidase is essential for manganese oxidation and laccase-like activity in *Pedomicrobium* sp. ACM 3067, Environ. Microbiol. 9 (2007) 944–953.
[23] C.N. Butterfield, A.V. Soldatova, S.W. Lee, T.G. Spiro, B.M. Tebo, Mn(II, III) oxidation and Mn_O2 mineralization by an expressed bacterial multicopper oxidase, Proc. Natl. Acad. Sci. U.S.A. 110 (2013) 11731–11735.
[24] Z. Zhang, Z. Zhang, H. Chen, J. Liu, C. Liu, H. Ni, C. Zhao, M. Ali, F. Liu, L. Li, Surface Mn(II) oxidation actuated by a multicopper oxidase in a soil bacterium leads to the formation of manganese oxide minerals, Sci. Rep. 5 (2015) 10895.
[25] J. Liu, L. Tan, J. Wang, Z. Wang, H. Ni, L. Li, Complete biodegradation of chlorpyrifos by engineered Pseudomonas putida cells expressing surface-immobilized laccases, Chemosphere 157 (2016) 200–207.
[26] W. Wang, Z. Zhang, H. Ni, X. Yang, Q. Li, L. Li, Decolorization of industrial synthetic dyes using engineered *Pseudomonas putida* cells with surface-immobilized bacterial laccase, Microb. Cell Fact. 11 (2012) 75.
[27] P.S. Daugherty, Protein engineering with bacterial display, Curr. Opin. Struct. Biol. 17 (2007) 474–480.
[28] X. Shao, Y. Gao, M. Jiang, L. Li, Deletion and site-directed mutagenesis of laccase from *Shigella dysenteriae* results in enhanced enzymatic activity and thermostability, Enzyme Microb. Tech. 44 (2009) 274–280.
[29] L.O. Martins, C.M. Soares, M.M. Pereira, M. Teixeira, T. Costa, G.H. Jones, A.O. Henriques, Molecular and biochemical characterization of a highly stable bacterial laccase that occurs as a structural component of the *Bacillus subtilis* endospore coat, J. Biol. Chem. 277 (2002) 18849–18859.
[30] J. Su, P. Bao, T. Bai, L. Deng, H. Wu, F. Liu, J. He, CotA, a multicopper oxidase from *Bacillus pumilus* WH4, exhibits manganese-oxidase activity, PloS One 8 (2013) e60573.
[31] J. Sambrook, D.W. Russell, Molecular Cloning: A Laboratory Manual, 3rd ed., Cold Spring Harbor Laboratory Press, Cold Spring Harbor, N.Y., 2011.
[32] F.C. Boogerd, J.P. de Vrind, Manganese oxidation by *Leptothrix discophora*, J. Bacteriol. 169 (1987) 489–494.
[33] Q. Li, Z. Yu, X. Shao, J. He, L. Li, Improved phosphate biosorption by bacterial surface display of phosphate-binding protein utilizing ice nucleation protein, FEMS Microbiol. Lett. 299 (2009) 44–52.
[34] Q. Li, H. Ni, S. Meng, Y. He, Z. Yu, L. Li, Suppressing *Erwinia carotovora* pathogenicity by projecting *N*-acyl homoserine lactonase onto the surface of *Pseudomonas putida* cells, J. Microbiol. Biotechnol. 21 (2011) 1330–1335.
[35] L. Li, D.G. Kang, H.J. Cha, Functional display of foreign protein on surface of *Escherichia coli* using N-terminal domain of ice nucleation protein, Biotechnol. Bioeng. 85 (2004) 214–221.
[36] I. Michalak, K. Chojnacka, K. Marycz, Using ICP-OES and SEM-EDX in biosorption studies, Mikrochim. Acta 172 (2011) 65–74.
[37] M. Villalobos, B. Toner, J. Bargar, G. Sposito, Characterization of the manganese oxide produced by *Pseudomonas putida* strain MnB1, Geochim. Cosmochim. Acta 67 (2003) 2649–2662.
[38] W. Yang, Z. Zhang, H. Chen, J. Liu, M. Ali, F. Liu, L. Li, Population structure of manganese-oxidizing bacteria in stratified soils and properties of manganese oxide aggregates under manganese-complex medium enrichment, PloS One 8 (2013) e73778.
[39] J. Sajiki, J. Yonekubo, Leaching of bisphenol A (BPA) to seawater from polycarbonate plastic and its degradation by reactive oxygen species, Chemosphere 51 (2003) 55–62.
[40] R. Loos, G. Hanke, G. Umlauf, S.J. Eisenreich, LC-MS-MS analysis and occurrence of octyl- and nonylphenol, their ethoxylates and their carboxylates in Belgian and Italian textile industry, waste water treatment plant effluents and surface waters, Chemosphere 66 (2007) 690–699.
[41] J. Tu, Z. Yang, C. Hu, Efficient catalytic aerobic oxidation of chlorinated phenols with mixed-valent manganese oxide nanoparticles, J. Chem. Technol. Biotechnol. 90 (2015) 80–86.
[42] C. Martin, P.F. Corvini, R. Vinken, C. Junghanns, G. Krauss, D. Schlosser, Quantification of the influence of extracellular laccase and intracellular reactions on the isomer-specific biotransformation of the xenoestrogen technical nonylphenol by the aquatic hyphomycete *Clavariopsis aquatica*, Appl. Environ. Microbiol. 75 (2009) 4398–4409.
[43] Y.C. Cao, G.Q. Sun, Y. Han, D.L. Sun, X. Wang, Determination of nitrogen, carbon and oxygen stable isotope ratios in N_2O, CH_4, and CO_2 at natural abundance levels by mass spectrometer, Acta Pedolog. Sin. 45 (2008) 249–258.
[44] M.W. Sutherland, B.A. Learmonth, The tetrazolium dyes MTS and XTT provide new quantitative assays for superoxide and superoxide dismutase, Free Radic. Res. 27 (1997) 283–289.
[45] N. Tominaga, S. Kohra, T. Iguchi, K. Arizono, A multi-generation sublethal assay of phenols using the nematode *Caenorhabditis elegans*, J. Health Sci. 49 (2003) 459–463.
[46] J.J. Morgan, Kinetics of reaction between O_2 and Mn(II) species in aqueous solutions, Geochim. Cosmochim. Acta 69 (2005) 35–48.
[47] S.G. Benner, D.W. Blowes, W.D. Gould, R.B. Herbert Jr., C.J. Ptacek, Geochemistry of a permeable reactive barrier for metals and acid mine drainage, Environ. Sci. Technol. 33 (1999) 2793–2799.
[48] J.H. Lee, D.W. Kennedy, A. Dohnalkova, D.A. Moore, P. Nachimuthu, S.B. Reed, J.K. Fredrickson, Manganese sulfide formation via concomitant microbial manganese oxide and thiosulfate reduction, Environ. Microbiol. 13 (2011) 3275–3288.
[49] P. Baldrian, Purification and characterization of laccase from the white-rot fungus *Daedalea quercina* and decolorization of synthetic dyes by the enzyme, Appl. Microbiol. Biotechnol. 63 (2004) 560–563.
[50] J. Du, J. Bao, Y. Liu, H. Ling, H. Zheng, S.H. Kim, D.D. Dionysiou, Efficient activation of peroxymonosulfate by magnetic Mn-MGO for degradation of bisphenol A, J. Hazard. Mater. 320 (2016) 150–159.
[51] T. Fukuda, H. Uchida, M. Suzuki, H. Miyamoto, H. Morinaga, H. Nawata, T. Uwajima, Transformation products of bisphenol A by a recombinant Trametes vilosa laccase and their estrogenic activity, J. Chem. Technol. Biotechnol. 79 (2004) 1212–1218.
[52] P.F.X. Corvini, A. Schaffer, D. Schlosser, Microbial degradation of nonylphenol and other alkylphenols – our evolving view, Appl. Microbiol. Biotechnol. 72 (2006) 223–243.
[53] Z.J. Lu, J. Gan, Oxidation of nonylphenol and octylphenol by manganese dioxide: kinetics and pathways, Environ. Pollut. 180 (2013) 214–220.
[54] A. Sinha, V.N. Singh, B.R. Mehta, S.K. Khare, Synthesis and characterization of monodispersed orthorhombic manganese oxide nanoparticles produced by *Bacillus* sp. cells simultaneous to its bioremediation, J. Hazard. Mater. 192 (2011) 620–627.
[55] I. Saratovsky, P.G. Wightman, P.A. Pasten, J.F. Gaillard, K.R. Poeppelmeier, Manganese oxides: parallels between abiotic and biotic structures, J. Am. Chem. Soc. 128 (2006) 11188–11198.
[56] E.V. Rokhina, K. Makarova, M. Lahtinen, E.A. Golovina, H.V. As, J. Virkutyte,

Ultrasound-assisted MnO_2 catalyzed homolysis of peracetic acid for phenol degradation: the assessment of process chemistry and kinetics, Chem. Eng. J. 221 (2013) 476–486.
[57] Q. Li, X. Huang, G. Su, M. Zheng, C. Huang, M. Wang, C. Ma, D. Wei, The regular/persistent free radicals and associated reaction mechanism for the degradation of 1,2,4-trichlorobenzene over different MnO_2 polymorphs, Environ. Sci. Technol. 52 (2018) 13351–13360.
[58] N. Miyata, Y. Tani, M. Sakata, K. Iwahori, Microbial manganese oxide formation and interaction with toxic metal ions, J. Biosci. Bioeng. 104 (2007) 1–8.
[59] Q. Luo, X. Yan, J. Lu, Q. Huang, Perfluorooctanesulfonate degrades in a laccase-mediator system, Environ. Sci. Technol. 52 (2018) 10617–10626.
[60] S. Zhang, L. Gutierrez, X.Z. Niu, F. Qi, J.P. Croue, The characteristics of organic matter influence its interfacial interactions with MnO_2 and catalytic oxidation processes, Chemosphere 209 (2018) 950–959.
[61] S. Zhu, X. Li, J. Kang, X. Duan, S. Wang, Persulfate activation on crystallographic manganese oxides: mechanism of singlet oxygen evolution for nonradical selective degradation of aqueous contaminants, Environ. Sci. Technol. 53 (2019) 307–315.
[62] Z. Zhao, J. Zhao, C. Yang, Efficient removal of ciprofloxacin by peroxymonosulfate/Mn_3O_4-MnO_2 catalytic oxidation system, Chem. Eng. J. 327 (2017) 481–489.
[63] L. He, T. He, S. Farrar, L. Ji, T. Liu, X. Ma, Antioxidants maintain cellular redox homeostasis by elimination of reactive oxygen species, Cell. Physiol. Biochem. 44 (2017) 532–553.
[64] L.A. Ioannou, G. Li Puma, D. Fatta-Kassinos, Treatment of winery wastewater by physicochemical, biological and advanced processes: a review, J. Hazard. Mater. 286 (2015) 343–368.
[65] A.R. Ribeiro, O.C. Nunes, M.F. Pereira, A.M. Silva, An overview on the advanced oxidation processes applied for the treatment of water pollutants defined in the recently launched Directive 2013/39/EU, Environ. Int. 75 (2015) 33–51.
[66] Y. Ren, L. Lin, J. Ma, J. Yang, J. Feng, Z. Fan, Sulfate radicals induced from peroxymonosulfate by magnetic ferrospinel MFe_2O_4 (M = Co, Cu, Mn, and Zn) as heterogeneous catalysts in the water, Appl. Catal. B 165 (2015) 572–578.
[67] X. Ding, K. Zhao, L. Zhang, Enhanced photocatalytic removal of sodium pentachlorophenate with self-doped Bi_2WO_6 under visible light by generating more superoxide ions, Environ. Sci. Technol. 48 (2014) 5823–5831.
[68] S. Mathew, T.E. Abraham, Z.A. Zakaria, Reactivity of phenolic compounds towards free radicals under in vitro conditions, J. Food Sci. Technol. 52 (2015) 5790–5798.
[69] A. Goyal, V.C. Srivastava, Treatment of highly acidic wastewater containing high energetic compounds using dimensionally stable anode, Chem. Eng. J. 325 (2017) 289–299.